EFFECT OF NICKEL EQUIVALENT ON HYDROGEN ENVIRONMENT EMBRITTLEMENT OF AUSTENITIC STAINLESS STEELS AT LOW TEMPERATURES

L. Zhang, M. Wen, M. Imade, S. Fukuyama and K. Yokogawa
National Institute of Advanced Industrial Science and Technology
Central 5, 1-1-1 East, Tsukuba, 305-0046, JAPAN

ABSTRACT

The Ni content of the austenitic stainless steels of Fe(10-20)Ni17Cr2Mo alloy (Ni-added alloy) and the N content of those of Fe11Ni17Cr2Mo(0.001-0.25)N alloy (N-added alloy), both based on type 316 stainless steel, were changed to study the effect of Ni equivalent on hydrogen environment embrittlement (HEE) of austenitic stainless steel. Tensile tests were conducted at a strain rate of 4.2×10^{-5}/s in hydrogen and helium at 1 MPa in the temperature range from 80 to 300 K. It was found that HEE of the alloys increased with decreasing temperature, reached a maximum at 200 K, and then decreased with further decreasing temperature. The content of strain-induced *α'* martensite increased with decreasing temperature and Ni equivalent. The susceptibility to HEE depended on Ni equivalent. Fracture surfaces observed by scanning electron microscopy revealed that hydrogen-induced fracture of Ni-added alloys occurred along *α'* martensite laths and twin boundaries and the fracture surfaces of N-added alloys showed transgranular fracture together with slip-plane fracture. HEE was mainly controlled by strain-induced *α'* martensite above 200 K, whereas it was controlled by hydrogen diffusion below 200 K. It was proposed that in Ni-added alloys HEE is completely controlled by *α'* martensite content. In N-added alloys, strain-induced *α'* martensite plays the primary role in HEE, but slip planarity plays a more important role in inducing HEE.

Introduction

The application of hydrogen as a foreseeable source of clean energy requires the development of a means for hydrogen storage and transportation. Austenitic stainless steels are expected to be good candidate materials for the structure of storage tanks, containers and line pipes for liquid hydrogen service. However, it has been shown that austenitic stainless steels suffer from hydrogen embrittlement (HE) at low temperatures. Stable stainless steels such as types 310 and 309 were susceptible to HE when they were hydrogen-charged cathodically and thermally [1-9], but they showed no HE in a hydrogen environment [4,5,10-14]. Metastable austenitic stainless steels such as types 301, 304 and 316, regardless of whether they were hydrogen-charged [2-6,11,15-27] or in a hydrogen environment [3-5,10,12-14,28-37], were all susceptible to HE. There were two main sources of HE of austenitic stainless steels. One is the strain-induced *α'* martensite observed during the deformation of metastable austenitic stainless steels [2-4,6,11,13,14,18,20,34-37,38]. It was proposed that the bcc structure of *α'* martensite is inherently more susceptible to hydrogen-induced cracking than the fcc structure, and it provides an effective short-circuit diffusion path for hydrogen due to the high diffusivity of hydrogen in it [38]. Another is the slip planarity [39] that occurs in the austenitic stainless steels with low stacking-fault energy (SFE). The low SFE suppresses cross-slip; thus, pile-ups with dense dislocations are formed, which initiates microcracks at the head of the pile-ups. It also enhances the dislocation transport of hydrogen, leading to high hydrogen concentrations at heterogeneous regions in the microstructure [8]. However, these two effects have not been distinguished in a material yet.

The main element of austenitic stainless steels is Ni, which improves resistance to HE by stabilizing austenite with respect to martensitic transformations and by increasing the SFE to promote cross-slip. Caskey studied HE of a wide variety of stainless steels including commercial and high-purity alloys [4]. It was found that HE of thermally hydrogen-charged alloys increased with decreasing temperature, reached a maximum at a certain temperature, and decreased with further decreasing temperature. The most serious HE occurred between 200 and 300 K. Ni improved HE by increasing austenite stability.

The addition of N also stabilizes austenite and improves resistance to HE. Hannula studied the effects of N on HE of cathodically hydrogen-charged type 304 austenitic stainless steels at room temperature [40]. It was proposed that N improves HE by stabilizing austenite, since N has minor effect on SFE [41,42]. However, N also promotes planar-slip by inducing a short-range order [41,43-46]. Thus, N and Ni play distinct roles in improving resistance to HE. It provides a way to distinguish HE due to strain-induced *α'* martensite from HE due to slip planarity.

The degree of austenite stability against strain-induced *α'* martensitic transformation and the tendency of forming austenite can be evaluated by an equation of Ni equivalent based on the equation by Hirayama [47]:

$$Ni_{eq} = Ni + 0.65Cr + 0.98Mo + 1.05Mn + 0.35Si + 12.6(C+N), \qquad (1)$$

where all elements are in weight fraction. Thus, HE can be correlated with Ni equivalent;, however, the effect of Ni equivalent on HE has not been studied until now.

The effect of Ni and N on hydrogen environment embrittlement (HEE) in austenitic stainless steels was examined to study the effect of Ni equivalent on HEE, and the roles of strain-induced *α'* martensite and slip planarity in HEE were identified in the temperature range from 80 to 300 K.

Experimental

The Ni content of the austenitic stainless steels of Fe(10-20)Ni17Cr2Mo alloy (Ni-added alloy) and the N content of those of Fe11Ni17Cr2Mo(0.001-0.25)N alloy (N-added alloy), both based on type 316 stainless steel, were changed to study the effect of Ni equivalent on HEE. The alloys were melted in a vacuum high-frequency induction furnace. After forging the materials into a round bar, the alloys were solution-annealed at 1373 K for 5 minutes, and then water-quenched. The alloys were machined into cylindrical tensile specimens with a gauge length of 20 mm and a diameter of 4 mm. The specimens were finally ground with sandpaper and polished with paste. Tensile tests were conducted in helium and hydrogen at 1 MPa in the temperature range from 80 to 300 K using the equipment specially developed in our laboratory for studying HEE at low temperatures [48]. The purity of the testing gases was 99.99999% in gas cylinder for hydrogen and 99.999% for helium. All tests were conducted at a strain rate of 4.2×10^{-5}/s to ensure a reasonable effect of hydrogen on the mechanical properties of the materials [38]. The fracture surface of the specimens after tensile tests was analyzed by scanning electron microscopy (SEM). The content of strain-induced *α'* martensite in austenite was measured by the magnetic method. The foil for transmission electron microscopy (TEM) was prepared from the specimen deformed by a strain of 10% at 200 K. The TEM foils were cut from the specimen and ground using sandpaper with water and final polishing and thinning were performed to perforation using a twin-jet technique in electrolyte of an 8% solution of $HClO_4$ in ethanol; then, the foils were observed using a Hitachi H-9000 TEM apparatus.

Results

Stress-strain curves for Fe11Ni17Cr2Mo alloy tested in hydrogen and helium at 80, 200 and 300 K are shown in Figure 1. No HEE appears at 80 K and 300 K, but hydrogen reduces elongation at 200 K considerably. HEE can be quantitatively described by the relative reduction of area (RRA), which is the reduction of area measured in hydrogen at 1 MPa relative to that in helium at 1 MPa (reduction of area in hydrogen / reduction of area in helium) [38]. There is no HEE when RRA equals 1, and HEE increases with decreasing RRA. The effect of Ni content and temperature on the RRA of Ni-added alloys is shown in Figure 2. RRA decreases with temperature, reaches a minimum at around 200 K and then increases with further decrease in temperature below a Ni content of 13 wt.%. Ni increases the RRA between 150 and 250 K and the increase is most significant at 200 K. No HEE is observed above a Ni content of 13 wt.%. The effects of N content and temperature on the RRA of N-added alloys are shown in Figure 3. The dependence of RRA on N is the same as that on Ni. The most significant increase in RRA occurred at 200 K, when N content is larger than 0.072 wt.%. It is clear that the addition of both Ni and N decreases the HEE sensitivity of the alloys significantly.

In order to understand the effects of N and Ni on HEE, we compare Ni-added alloys with N-added ones. The effects of Ni equivalent on both the ferrite equivalent and RRA of Ni- and N-added alloys at 200 K are shown in Figure 4. The ferrite equivalent corresponds to *α'* martensite content in the specimen tested in helium. The difference between the ferrite equivalent of Ni-added alloy and that of N-added alloy at a given Ni equivalent is very small; thus, it is obvious that Ni equivalent correctly predicts the austenite stability. However, these two kinds of alloys have different RRAs. For Ni-added specimens, when Ni equivalent is above 27.2%, HEE is not observed. For N-added specimens, HEE is always observed, although it decreases with increasing Ni equivalent.

Fracture surfaces of Fe11Ni17Cr2Mo alloy fractured in helium at 200 K are shown in Figure 5. It is evident that the fracture mode is dimple rupture. The fracture mode of both Ni- and N-added alloys tested at all temperatures in helium is the dimple rupture mode.

Fracture modes for both Ni- and N-added alloys tested in hydrogen at 200 K are all brittle transgranular fracture, but their characters are different. A SEM fractograph of Fe11Ni17Cr 2Mo alloy tested in hydrogen at 200 K is shown in Figure 6. The brittle and transgranular fracture is observed in Figure 6(a), which indicates that the crack first originates from the surface of the specimen, and then propagates inside the matrix of the specimen. Figure 6(b) shows a magnified image of area A. Slip traces are shown on the fracture surface. SEM fractograph of Fe11Ni17Cr2Mo0.24N alloy tested in hydrogen at 200 K is shown in Figure 7. Figure 7(a) shows that the crack also originates from the surface, and the initial crack is more obvious than that in Fe11Ni17Cr2Mo alloy. Figure 7(b) shows a magnified image for area B. There are more microcracks on the fracture surface, which may be the traces of plastic deformation. The slip steps seem to be parallel to one set of steps forming the sawtooth profile, thus suggesting that steps may be formed by the {111} slip planes in austenite. The fractograph shows the obvious tendency of planar-slip in austenite, which is due to the effect of hydrogen on the dislocation motion [11,49,50].

The TEM microstructure of Fe11Ni17Cr2Mo alloy deformed by a strain of 10% in helium at 200 K is shown in Figure 8. α' martensite and ε martensite have been observed. Selected-area diffraction, which is not shown here, indicates that the band structure is ε martensite and the lath structure is α' martensite. α' martensite is formed at the intersection between ε martensite bands, and grows up along the {111} slip planes in austenite, as reported by Han et al. [48].

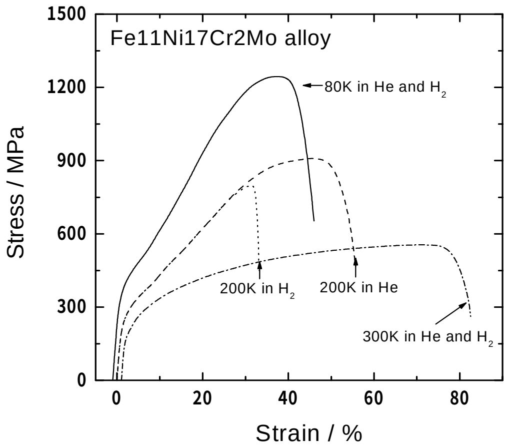

Figure 1. Stress-strain curves for Fe11Ni17Cr2Mo alloy tested in hydrogen and helium at 80, 200 and 300 K.

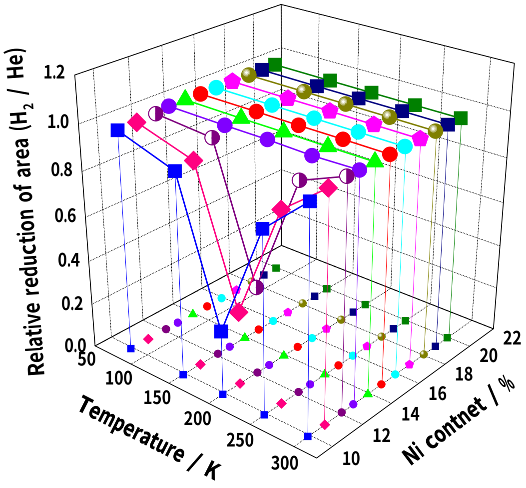

Figure 2. Effects of Ni content and temperature on RRA of Ni-added alloys.

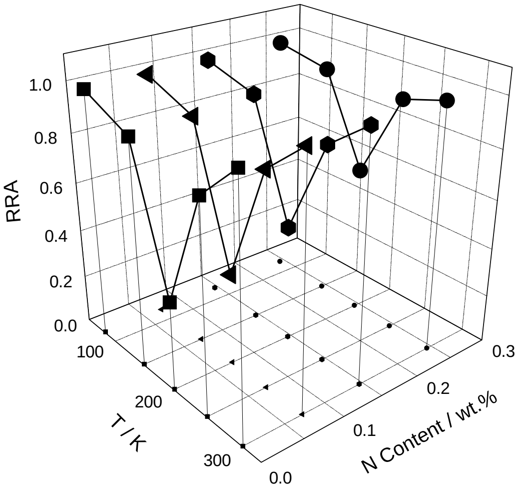

Figure 3. Effects of Ni content and temperature on RRA of N-added alloys.

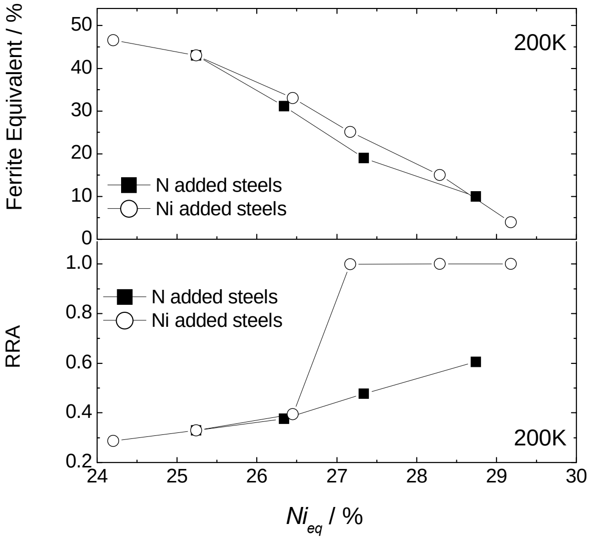

Figure 4. Effects of Ni equivalent on ferrite equivalent and RRA of Ni- and N-added alloys tested at 200 K.

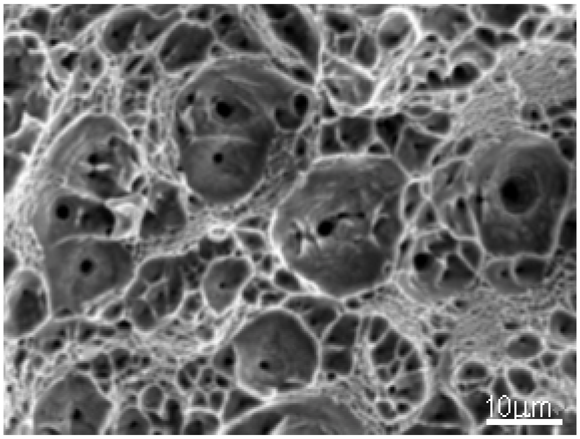

Figure 5. SEM fractograph of Fe11Ni17Cr2Mo alloy fractured in helium at 200 K.

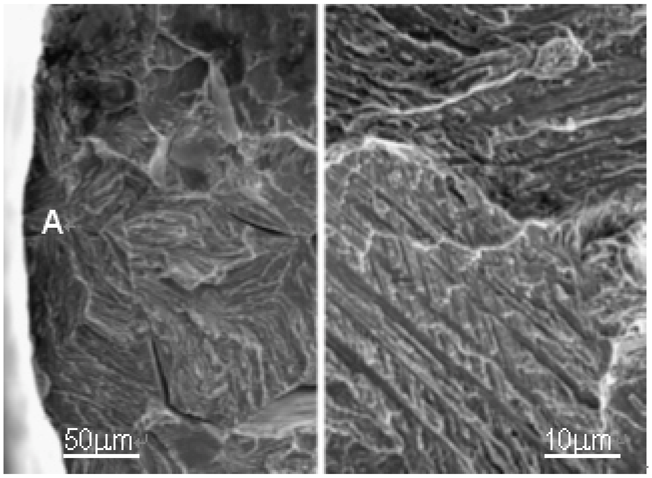

Figure 6. SEM fractograph of Fe11Ni17Cr2Mo alloy tested in hydrogen at 200 K ((a) origin of crack and magnified image of area A).

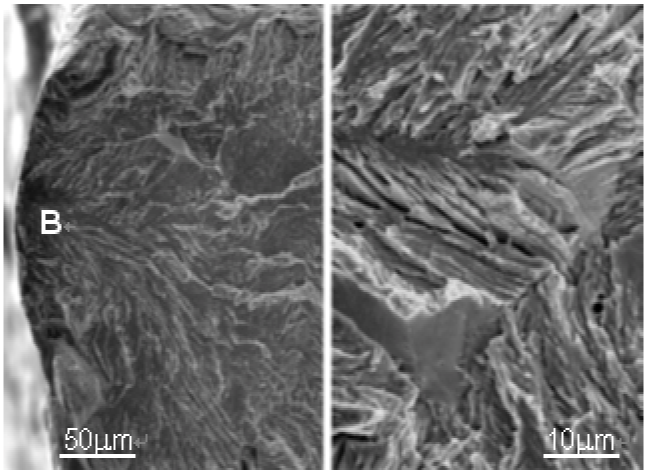

Figure 7. SEM fractograph of Fe11Ni17Cr2Mo0.24N alloy tested in hydrogen at 200 K ((a) origin of crack and (b) magnified image of area B).

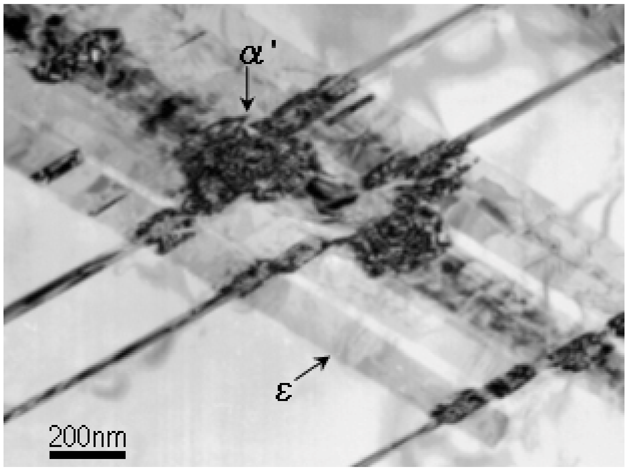

Figure 8. TEM microstructure of Fe11Ni17Cr2Mo alloy deformed in helium at 200 K with 10% strain.

Discussions

Type 316 stainless steels are austenitic alloys with good corrosion resistance and mechanical properties. The steels have a high SFE due to their high Ni and Mo contents, which promotes cross slip. However, the steels still suffer from hydrogen-induced fracture as observed in this study. SEM observations on fracture surfaces revealed that transgranular fracture occurs along *α'* martensite laths and TEM observations showed that strain-induced *α'* martensite is formed at the intersections of the microscopic slip bands in the grains. It is considered that strain-induced *α'* martensite plays a key role in hydrogen-induced crack growth in the alloys.

The RRA of both Ni- and N-added alloys decreases with temperature, reaches a minimum at 200 K, and then increases with further decreasing temperature, as shown in Figure 2. This is in good accordance with the observations of the temperature dependence of type 316 steel thermally hydrogen-charged [4] and in a hydrogen environment at 1 MPa [38], where the maximum HE occurred at 200 K. It was originally proposed by Troiano [51] and then supported by others [14,36,52,53] that HE is controlled by hydrogen transportation and accumulation in the triaxial tensile region ahead of a crack tip. The transportation of hydrogen to a crack tip depends on the temperature and microstructure [54,55]. Generally, a small amount of hydrogen is sufficient to cause hydrogen-induced damage because it can magnify its effect by diffusion to the potential cracking region where triaxial stress is high.

The bcc *α'* martensite has a much higher diffusion coefficient of hydrogen than fcc austenite [23], which provides an effective short-circuit path for hydrogen transportation [38]. At temperatures above the maximum HEE temperature, the content of strain-induced *α'* martensite increases rapidly with decreasing temperature, as shown in Figure 3. The transportation of hydrogen and consequently the susceptibility to HEE are thus controlled by the amount of strain-induced *α'* martensite in the alloy. At temperatures below the maximum HEE temperature, since the diffusion of hydrogen decreases rapidly with temperature, the accumulation of hydrogen in the region of high triaxial stress becomes more and more difficult in this temperature range. Thus, HEE is controlled by the slow process of hydrogen diffusion below the maximum HEE temperature. It decreases with temperature until it vanishes.

Caskey studied a wide variety of stainless steels including commercial and high-purity alloys [4]. It was found that HEE of Fe-Cr-Ni alloys was dependent on Ni content. There was a marked improvement in resistance to HEE in the composition range of Ni from 8 to 14% in 69 MPa hydrogen at even room temperature. The present study revealed that the content of strain-induced *α'* martensite decreases with increasing Ni equivalent, as shown in Figure 4, indicating that austenite can be stabilized by increasing Ni equivalent. This study also revealed that fracture occurred in strain-induced martensite, as shown in the fracture surfaces. It is thus expected that HEE can be suppressed or RRA can be increased by increasing Ni equivalent.

Although both N and Ni can stabilize austenite, they showed distinct roles in improving resistance to HE, as shown in Figure 4. Ni improves resistance to HE by stabilizing the austenite phase with respect to martensitic transformations and by increasing SFE to promote cross-slip. N, however, not only increases the stability of the austenite phase with respect to martensitic transformations, but also results in serious slip planarity by inducing a short-range order. As is shown in Figure 7, microcracks were formed along slip traces in 316LN-4, indicating a slip-planarity-induced damage.

Conclusions

The Ni content of the austenitic stainless steels of Fe(10-20)Ni17Cr2Mo alloy and the N content of those of Fe11Ni17Cr2Mo(0.001-0.24)N alloy, both based on type 316 stainless steel, were changed to study the effect of Ni equivalent on HEE. Tensile tests were conducted at a strain rate of 4.2×10^{-5} /s in hydrogen and helium at 1 MPa in the temperature range from 80 to 300 K. The content of strain-induced *α'* martensite in austenite was measured by the magnetic method. The fracture surface of the specimen after tensile tests was analyzed by SEM and the microstructure was analyzed by TEM. The following conclusions were drawn on the basis of this work:

1. HEE increases with decreasing temperature, reaches a maximum at 200 K, and decreases with further decreasing temperature until it completely vanishes.

2. HEE is correlated with Ni equivalent. The content of strain-induced *α'* martensite increased with decreasing temperature and Ni equivalent. The susceptibility to HEE increased with decreasing Ni equivalent.

3. Hydrogen-induced fracture of Ni-added steels occurred along *α'* martensite laths and twin boundaries. HEE is controlled by *α'* martensite above the maximum HEE temperature, whereas it is controlled by the diffusion of hydrogen below the maximum HEE temperature.

4. Brittle transgranular fracture, together with slip-plane fracture, was observed in N-added alloys. Although strain-induced *α'* martensite plays the primary role in HEE, slip planarity plays an important role in inducing HEE when N is increased in the alloys.

References

1. Whiteman, M. B. and Troiano, A. R., Corrosion, **21**, 53(1965).
2. Holzworth, M. L., Corrosion, **25**, 107(1969).
3. Hosoya, Y., Inoue, A., Masumoto, T., J. Iron Steel Inst. Japan, **64**, 769(1978).
4. Caskey, Jr. G. R., Environment degradation of engineering materials in hydrogen, ed. by Louthan, M. R., McNitt, Jr. R. P., Sisson, Jr. R. D., Blacksburg, VA: Virginia Polytechnic Institute; 1981, p. 283.
5. Eliezer, D., Chakarapani, D. G., Alstetter, C. J., Pugh, E. N., Metall. Trans. A, **10A**, 935(1979).
6. Liu, R., Narita, N., Altstetter, C. J., Birnbaum, H., Pugh, E. N., Metall. Trans. A, **11A**, 1563(1980).
7. Ma, L., Liang, G., Li, Y., adv. Cryogen Eng. (Mater.), **38**, 77(1992).
8. Abraham, D. P., Altstetter, C. J., Metall. Trans. A, **26A**, 2849(1995).
9. Abraham, D. P., Altstetter, C. J., Metall. Trans. A, **26A**, 2859(1995).
10. Benson, R. B. Jr., Dann, R. K., Roberts, L. W. Jr., Trans. Metall. Soc. A.I.M.E., **242**, 2199(1968).
11. Hañninen, H., Hakkarainen, T., Metall. Trans. A, **10A**, 1196(1979).
12. Walter, R. J., Chandler, W. T., Mater. Sci. Engng., **8**, 90(1971).
13. Singh, S., Altstetter, C. J., Metall. Trans. A, **13A**, 1799(1982).
14. Perng, T. P., Altstetter, C. J., Metall. Trans. A, **18A**, 123(1987).
15. Vennett, R.M., Ansell, G. S., Trans. Am. Soc. Metals, **60**, 242(1967).
16. Lagneborg, R., J. Iron Steel Inst., March, 363(1969).
17. Okada, H., Hosoi, Y., Abe, S., Corrosion, **26**, 183(1970).
18. Ohtani, N., Asano, S., Fujishima, Y., Yamamasu, Y., J. Japan Inst. Metals, **37**, 746(1973).
19. Thompson, A. W., Metall. Trans. A, **4**, 2819(1973).
20. Hañninen, H. and Hakkarainen, T., Corrosion, 1980, **36**, 47.
21. Holbrook, J. H., Hydrogen effect in materials, ed. by Bernstein, I. M., Thompson, A. W., Warrendale: AIME, 1981, p. 655.
22. Stolz, R. E., Mooy, N. R., Perra, M.W., Metall. Trans. A, **14A**, 1528(1983).
23. Nelson, H. G., Treatise Mater. Sci. Technol., **25**, 275(1983).
24. Eliezer, D., J. Mater. Sci., **19**, 1540(1984).
25. Eliezer, D., J. Mater. Sci., **25**, 2532(1990).
26. Toribio, J. Fusion Engng. Des., **16**, 337(1991).
27. Huang, J. H., Alstetter, C. J., Metall. Trans. A, **26A**, 1079(1995).
28. Mills, R. L., Edeskuty, F. J., Chem. Engng. Prog., **52**, 477(1956).
29. Walter, R. J., Jewett, R. P., Chandler, W. T., Mater. Sci. Engng., **5**, 98(1969).
30. Vennett, R. M., Ansell, G. S., Trans. Am. Soc. Metals, **62**, 1007(1969).
31. Vandervoort, R. R., Metals Engng. Q., **12**, 10(1972).
32. Louthan, Jr. M. R., Hydrogen in metals, ed. by Bernstein, I. M., Thompson, A. W., AIME; 1976, p. 53.
33. Fujiwara, K., Sugie, K., Proc. of the international corrosion forum, Houston: sponsored by the National Association of Corrosion Engineering; 1982, p. 188.
34. Schuster, G., Altstetter, C. J., Metall. Trans. A, **14A**, 2077(1983).
35. Schuster, G., Altstetter, C. J., Metall. Trans. A, **14A**, 2085(1983).
36. Perng, T. P., Altstetter, C. J., Metall. Trans. A, **19A**, 145(1988).
37. Han, G., He, J., Fukuyama, S., Yokogawa, K., Proc. 16th int. cry. Eng. Cry. mater., ed. by Haruyama, T., Mitsui, T., Yamafuji, K., Kitakyushu, Japan, 1986, p. 1919.
38. Han, G., He, J., Fukuyama, S., Yokogawa, K., Acta Metall., **46**, 4559(1998).
39. Symons, D. M., Metall. Mater. Trans. A, **28A**, 655(1997).
40. Hannula, S. P., Hañninen, H., Tahtinen, S., Metall. Trans. A, **15A**, 2205(1984).
41. Swann, P. R., Corrosion, **19**, 102(1963).
42. Douglas, D., Thomas, G., Roser, W. R., Corrosion, **20**, 15(1964).
43. Ningshen, S., Uhlemann, M., Schneider, F., Corrosion Sci., **43**, 2255(2001).
44. Uhlemann, M., Shehata, M. F., Mummert, K., Mater. Sci. Forum, **318-3**, 523(1999).
45. Gavriljuk, V. G., Berns, H., Escher, C., Mater. Sci. Eng. A, **271**, 14(1999).
46. Tseng, C. M., Liou, H. Y., Tsai, W. T., Mater. Sci. Eng. A, **344**, 190(2003).
47. Hirayama, T., Ogirima, M., J. Jpn. Inst. Met., **34**, 507(1970).
48. Han, G., He, J., Fukuyama, S., Yokogawa, K., Rev. Sci. Instrum., **68**, 4232(1997).
49. Gaskey, G. R., Script Metall., **11**, 1077(1977).
50. Robertson, I. M., Birnbaum, H. K., Acta Metall., **34**, 353(1986).
51. Troiano, A. R., ASM Trans., **52**, 54(1960).
52. Oriani, R. A., Josephic, P. H., Acta Metall., **25**, 797(1977).
53. Symons, D. M., Thompson, A. W., Metall. Trans. A, **27A**, 101(1996).
54. Donovan, J. A., Metall. Trans. A, **7A**, 1677(1976).
55. Hirth, J. P., Metall. Trans. A, **11A**, 861(1980).